https://dx.doi.org/10.1016/j.conbuildmat.2020.119408

Strength development and microstructure characteristics of artificial concrete pillar considering fiber type and content effects

Shuai Cao[1,2,3]*, Di Zheng[1,2], Erol Yilmaz[4]*, ZhenYu Yin[3]*, GaiLi Xue[1,2], FuDou Yang[1,2,5]

[1]*State Key Laboratory of High-Efficient Mining and Safety of Metal Mines of Ministry of Education, University of Science and Technology Beijing, Beijing 100083, China*
[2]*School of Civil and Resource Engineering, University of Science and Technology Beijing, Beijing 100083, China*
[3]*Department of Civil and Environmental Engineering, The Hong Kong Polytechnic University, Hung Hom, Kowloon, Hong Kong, China*
[4]*Department of Civil Engineering, Geotechnical Division, Recep Tayyip Erdogan University, Fener, Rize TR53100, Turkey*
[5]*Zijin Tungsten Industry Group Corporation Ltd., Nanwenhe Tungsten Mine, Yunnan 8161003 China*

**Corresponding authors:* sandy_cao@ustb.edu.cn (S. Cao); erol.yilmaz@erdogan.edu.tr (E. Yilmaz); zhenyu.yin@polyu.edu.hk (ZY. Yin)

Abstract: The artificial concrete pillar (ACP) replacement technique is a safe and reliable method to safely mine orebody pillar in room and pillar mining. In contrast to traditional ore pillar, artificial pillar has recently received significant attention due to its applicability, stability and cost benefits. This study deals the influence of fiber type and content on uniaxial compressive strength (UCS) and microstructure characteristics of fiber-reinforced concrete (FRC) considered as an effective artificial pillar. A total of 3 non-FRC (NFRC) and 27 FRC samples reinforced with glass, polypropylene (PP), and polyacrylonitrile (PAN) fibers at a content of 0 wt.%, 0.4 wt.%, 0.8 wt.% and 1.2 wt.% were manufactured for examining their strength properties. After UCS testing, some microstructure tests including computed tomography scan and scanning electron microscopy coupled with energy dispersive X-ray spectroscopy were done to better explore the morphology of FRC. Results illustrate that: (1) The UCS values of all FRC samples first increase and then decrease with increasing fiber content. The UCS increment ratio in FRC steadily decreases as the fiber content increases. (2) PP fiber was more effective than both glass and PAN fibers in increasing peak strain and strength performance. This was mainly because of an improved bonding quality within the matrix which allows to decrease the water absorption of FRC. Overall, the peak strain increases linearly with increasing fiber content. Finally, the findings of this study can offer a substantial reference in design and application of FRC to be used as artificial pillar in underground mines.

Keywords: Artificial concrete pillar; fiber-reinforced concrete; fiber reinforcement; strength properties; computed tomography; microstructure characteristics

1. Introduction

Room-and-pillar is an underground mining method in which ore is extracted across a horizontal plane, forming horizontal arrays of rooms and pillars [1]. To do this, 'rooms' of the ore are excavated while 'pillars' of the undistributed ore are left to support the hanging wall [2]. Room-and-pillar mining can be lucrative since it lessens the risk of surface subsidence and allows us to expand underground operations by fully mechanized mining technology when compared to other underground mining methods [3-5]. But, because substantial parts of the ore can have to be left behind, recovery and profits can be low radically [6]. This method is typically used in flat-bedded deposits of limited thickness, such as metals (e.g., gold, zinc, lead and copper), coal, salt, and limestone [7]. Although remaining pillars improved the stability of the stope, loss of a large number of orebody pillars leads to a waste of ore resources [8]. Pillar stability is crucial to the secure and economic operation of an underground mine since pillar failure can negatively affect mining by creating unstable roof and floor conditions [9]. Considering the impact of pillar stability, various research efforts through empirical, theoretical and numerical simulation methods have been made to evaluate the stability of pillars [10-12].

Indeed, several field and laboratory works have well indicated the usage of artificial supports to better enhance the design, durability and load carrying capacity of pillars [13-15]. Reinforcement is most often used in the mining industry for improving the strength and stability of pillars. Li et al. [16] developed an artificial expandable pillar (using a chemical mixture that expands when water is introduced) for hard rock pillar mining. It is clearly found that expandable pillars can stabilize an excavation with small roof deformation. To control roof deformation, rock bolting technique was used at room and pillar in Upper Silesian Coal Basin [17]. Yu et al. [18] considered the progressive pillar size reduction and the confining behaviors of peeled coal debris and proposed an improved method for long-term stability appraisal of strip mining and pillar. Sun et al. [19] used the cementitious backfill system to mine coal pillar in Qishan Coal Mine, China. Hauquin et al. [20] found a more accurate analytical method for calculating vertical stress on pillars of irregular size by using a finite code, which offers a better guess than existing methods. Ghasemi et al. [21] studied a relationship between pillar size and five parameters (e.g., depth of cover, mining height, panel width, roof strength rating and loading conditions) by the cosine amplitude method. Results have shown that the most effective parameter on pillar size is the loading conditions. Using the concrete replacement method to orebody pillars was a safe mining method in room and pillar mining.

Several researchers have conducted the mechanical properties of concrete [22-24]. Mostly, concrete is made up of water, binder, sand and aggregate gravels. However, researches have showed that this type of concrete easily breaks and loses its strength development under external load surcharges [25, 26]. Hence, some researchers have used additive materials (e.g., steel and polypropylene fibers and rubber) to prepare fiber-reinforced concrete (FRC) which eliminates the earlier-mentioned problems and enhances its early and late mechanical strength acquisitions. Until now, the uniaxial compressive strength, flexural bending and microstructural tests have been the main focus on strength characteristics of FRC materials [27-32]. Le et al. [33] found that the formation and propagation of cracks occurred under progressive loading within FRC were significantly influenced by fiber bridging mechanisms. Usman et al. [34] proved that utilization of steel fiber had a minute effect on compressive strength, whereas it eloquently improved its ductility and enhanced the post-peak behavior of concrete. Besides, fiber diameter, fiber volume fraction, aggregate diameter and aggregate volume fraction knowingly influenced the process of chloride diffusion within FRC materials [35, 36]. The bonding between fiber and cement matrix is smoothly enhanced by a full replacement of ordinary Portland cement with expansive cement which can thus improve the strength properties of hybrid-FRC materials [37].

Non-destructive testing is a vital technique to study fiber reinforcement and the distribution of pores and cracks within rocks, cemented paste/tailings backfill and concrete [38-49]. Jalal et al. [50] found that ultrasonic pulse velocity (UPV) can be used to better forecast the compressive strength performance of rubberized concrete. Another non-destructive testing technique is nuclear magnetic resonance (NMR), which allows us to authenticate the unique structure of the materials and to identify its carbon-hydrogen framework. In comparison with UPV and NMR, computed tomography (CT) scan can more accurately obtain the characteristics of internal defects of cementitious or rock materials due to its advantages of high x-ray energy and strong penetrating ability [51-57]. Vicente et al. [58] observed that differences in the behavior of both series were mainly related to their fiber content and, to a lesser extent, to their fiber orientation which is clearly determined by means of CT scan technique. Stelzner et al. [59] found that the addition of fibers leads to a faster and deeper migration of the drying front by means of X-ray CT and ^{1}H-NMR, which is the most common atom used in NMR spectroscopy. One can show that industrial CT technique has clear advantages in analyzing the internal sections and 3D reconstruction of cementitious materials such as cements, mortars and concretes.

Indeed, the recovery of ore pillars is a huge technical problem, and its mining safety risk is extremely high in room and pillar mining. Fig. 1a shows the room-and-pillar mining method implemented in a mine located in Yunnan province, China. There are lots of ore pillars left in underground trial stopes. The main feature of these ore pillars is the high grade which is 5-10 times higher than ordinary mineral grade. With a significant decrease in orebody grade, pillar mining is considered in this mine for improving the overall ore grade. Engineers originally tried to prepare numerous artificial concrete pillar (ACP) by mixing large pieces of waste rock and cement. However, these artificial pillars were harshly deformed and cracked in a short period of time and then failed to mine orebody pillar, as shown in Fig. 1b.

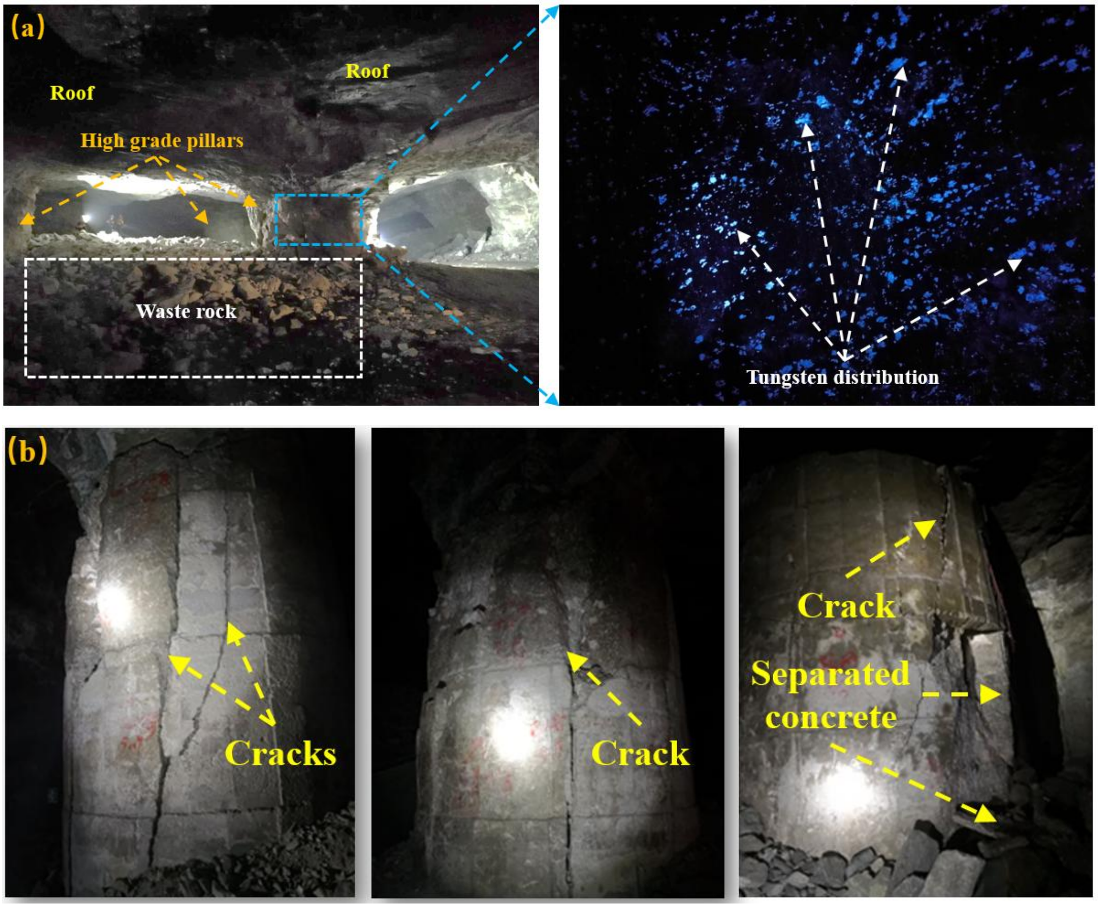

Fig. 1 Photos of a) ore pillar and grade distribution in a stope and b) failures of artificial concrete pillar

Despite the significant progress made in understanding the strength behavior in FRC systems, all these works have ignored the use of FRC as artificial concrete pillar in underground mines by investigating its fiber reinforcing effects. There is hence a need to address this research gap. The originality of this study consists in the assessment of the influence of fiber type and content on mechanical strength development and microstructure characteristics of artificial concrete pillar. The core parameters investigated during experimental testing are fiber type (e.g., glass, PP and PAN fibers) and fiber content (e.g., 0 wt.%, 0.4 wt.%, 0.8 wt.% and 1.2 wt.%). A total of 30 FRC samples were manufactured first and then subjected to unconfined compressive strength tests, computed tomography scan and SEM-EDS tests. It is assumed that FRC can be improved with different fiber types and contents and acts as the main pillar used for the safe extraction of valuable minerals from underground mines without causing any casualties.

2. Materials and methods

2.1 Materials

Tap water, cement, sand, gravels and fibers with different mix proportions were utilized to prepare FRC samples. In this study, ordinary Portland cement PC 42.5R was selected as a main hydraulic cement and its chemical composition was summarized in Table 1. A hydraulic cement is indeed produced by milling Portland cement clinker together with gypsum. It is typically classified as PC 42.5, 'PC' is the symbol for ordinary Portland cement while the number 42.5 shows the minimum desired strength value achieved within 28 days. The 'R' indicates that the cement is early strength cement.

Table 1 Chemical composition of ordinary Portland cement PC 42.5R

Chemical composition	SiO_2	Fe_2O_3	Al_2O_3	MgO	CaO	SO_3	K_2O
Content (%)	20.1	2.91	5.11	1.57	61.8	1.98	0.37

Natural river medium quartz sand was used as a fine aggregate and its fineness modulus was about 2.5. The grain size of natural river sand ranges between 90 microns to 2.36 mm. Gravels were crushed with a grain diameter of 5-12mm. Note that any sand or gravel can be used for construction, depending on its grain-size and composition, stone type and surface structure.

To illustrate the effects of fiber/matrix interaction on strength performance of FRC, numerous fibers such as glass, polypropylene (PP) fiber and polyacrylonitrile (PAN) fibers were selected as additives (Fig. 2). Glass fiber is a material consisting of very fine fibers of glass. PP is a thermoplastic polymer used in a wide variety of applications and produced via chain-growth polymerization from the monomer propylene. PAN is a synthetic, semi-crystalline organic polymer resin, with the linear formula. Though it is thermoplastic, it melts above 300℃ if the heating rates are 50℃ per minute or above.

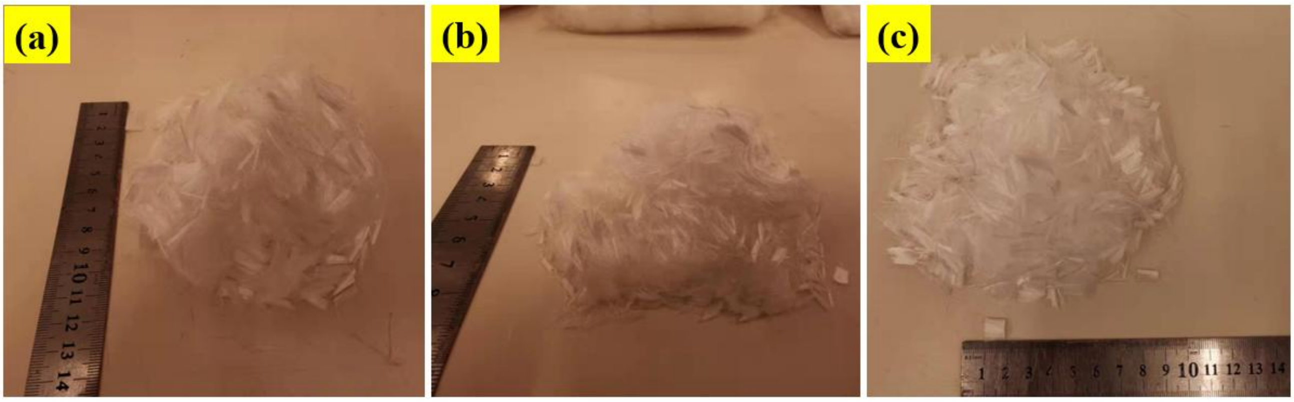

Fig. 2 Photos of different fibers used during the experiments: a) glass; b) PP, and (c) PAN

The basic parameters of the fibers used was listed in Table 2. Tap water was used to homogenously mix hydraulic cement, sand, gravels and fibers. Tap water can appear cloudy, often mistaken for mineral impurities in water, and caused by air bubbles coming out of solution due to change in the temperature or pressure. Note that chemical composition of tap water was not considered in this study.

Table 2 Basic parameters of different fibers used during the experiments

Fiber type	Length (mm)	Density (g/cm^3)	Diameter (μm)	Tensile strength (MPa)	Elastic modulus (GPa)	Elongation rate (%)
Glass	12	2.02	13-25	369	4.89	36.5
PP	12	0.91	18-68	398	3.85	28
PAN	12	0.91	28-72	736	4.68	30

2.2 Preparation of FRC samples

In this study, fiber type and content are two main considerations. The fiber content was set to 0 wt.%, 0.4 wt.%, 0.8 wt.% and 1.2 wt.%, respectively. The fiber reinforced concrete slurry was prepared based on cement/water/sand/gravel mix ratio was 1/0.7/2.51/3.08 and thoroughly mixed for at least 5 minutes. Subsequently, the slurry was poured into plastic cylinder molds with a diameter of 50 mm and a height of 100 mm. The tested FRC samples were placed within a standard temperature (25-32°C) and humidity (67-90%) curing box. The curing time for all FRC samples is set to 14 days. The surface flatness of FRC samples was measured as ±0.02 mm using a height gauge run across the surface of the part if only the reference feature is held parallel. Fig. 3 shows the preparation processes of FRC samples during the experiments in accordance with GB 50152-92 and JGJ 55-2011 [60].

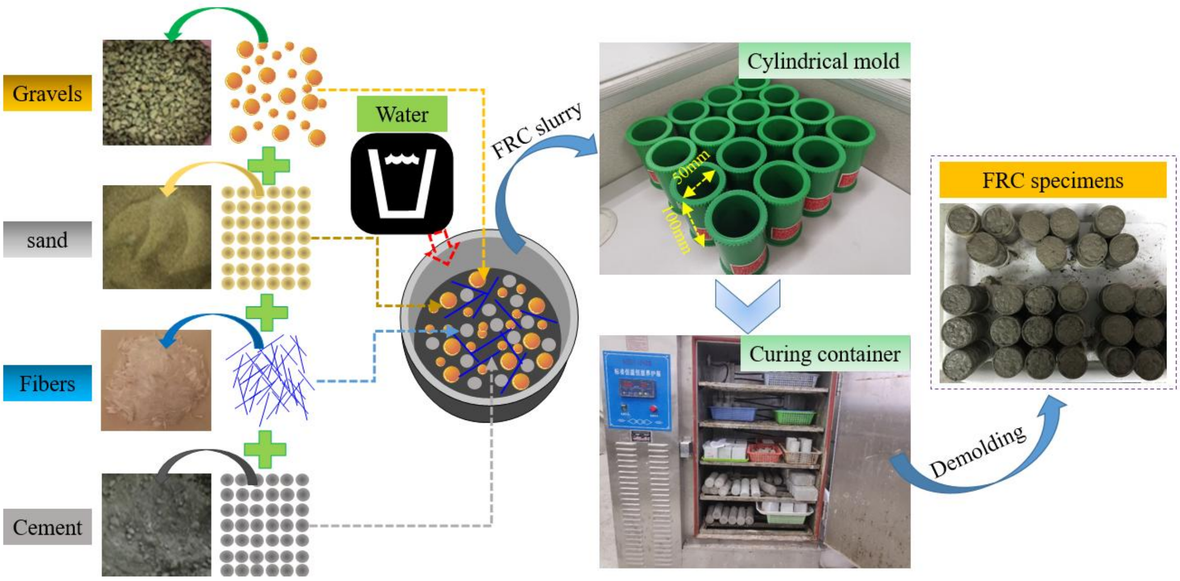

Fig. 3 The preparation processes of FRC samples used during the experiments

Indeed, the majority of field works, especially those in the mining sector, have not well addressed the influence of artificial pillars on both local and regional support in underground mines. To end up this gap, a field investigation was undertaken on FRC materials used as artificial pillar. The PP fiber, cement, river sand, gravel and tap water were added into the mixing boxes and mixed at least 5 minutes, then the FRC slurry was transported through the pipeline and pumped into the pre-built mold. The underground temperature and humidity were 25℃ and 80%, respectively. Fig. 4 demonstrates the field preparation and implementation steps of artificial concrete pillar in the underground mines.

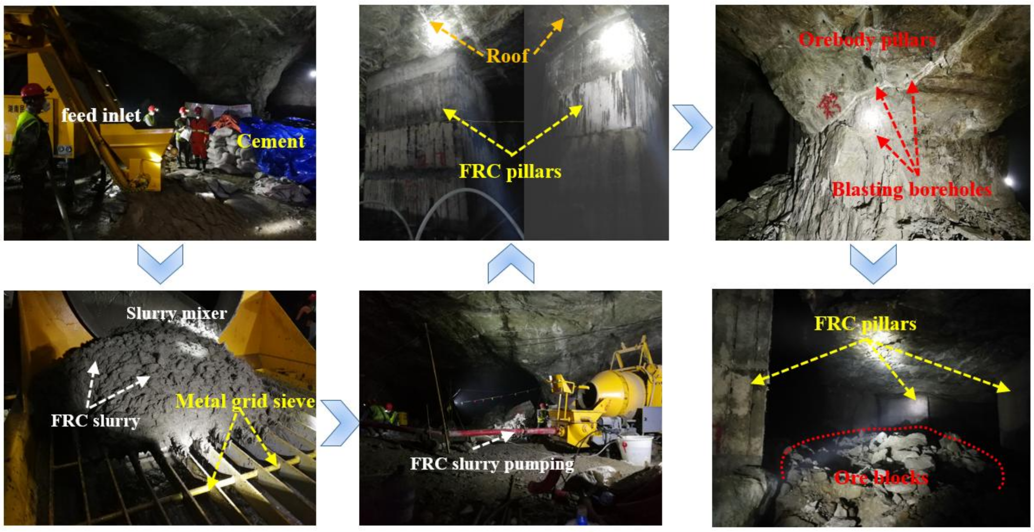

Fig. 4 Field preparation and implementation steps of FRC used as artificial pillar

Table 3 lists the mix proportions of FRC matrix to be used as artificial concrete pillar in underground mines, accompanying with control sample which does not contain any fiber. Taking sample G-0.4 as an example, G represents glass fiber, 0.4 represents a fiber content of 0.4 wt.%.

Table 3 A summary of the mix proportions of NFRC and FRC samples

Specimen ID	Cement (kg/m^3)	Water (kg/m^3)	Sand (kg/m^3)	Gravel (kg/m^3)	Fiber content (kg/m^3)
NFRC	329	231	826	1012	0
G-0.4	329	231	826	1012	9.592
G-0.8	329	231	826	1012	19.184
G-1.2	329	231	826	1012	28.776
PP-0.4	329	231	826	1012	9.592
PP-0.8	329	231	826	1012	19.184
PP-1.2	329	231	826	1012	28.776
PAN-0.4	329	231	826	1012	9.592
PAN-0.8	329	231	826	1012	19.184
PAN-1.2	329	231	826	1012	28.776

2.3 Uniaxial compressive strength testing

According to the Chinese standard GB/T1767-1999, the uniaxial compressive strength (UCS) tests of FRC samples were done for obtaining their mechanical strength properties. A loading equipment named WDW-100 from the Material Centre of University of Science and Technology Beijing was chosen in this study, which was continuously loaded at a constant speed of 0.5mm/min. To decrease experimental errors, each group of UCS testing contains at least three samples, and the average stress-strain values are obtained for evaluation of the ultimate analysis. Note that experimental data could be recorded and stored in the computer during the whole loading process.

2.4 Computed tomography scan testing

IPT 61 series of industrial computed tomography (CT) scan non-destructive testing system from Granpect Company Ltd., as shown in Fig. 5, was used to explore microscopic parameters, such as pores and cracks in FRC samples. The CT test system gears include: X-ray source, detector, high precision machinery of multiple freedom degrees and electrical control, system control and image processing computer, system control module, data acquisition module, image reconstruction module and image processing module, safety interlock and warning. The basic CT scan parameters were listed as follows: spatial resolution is 2.5 LP/mm, density resolution is 0.5% and the X-ray energy is 6 MeV.

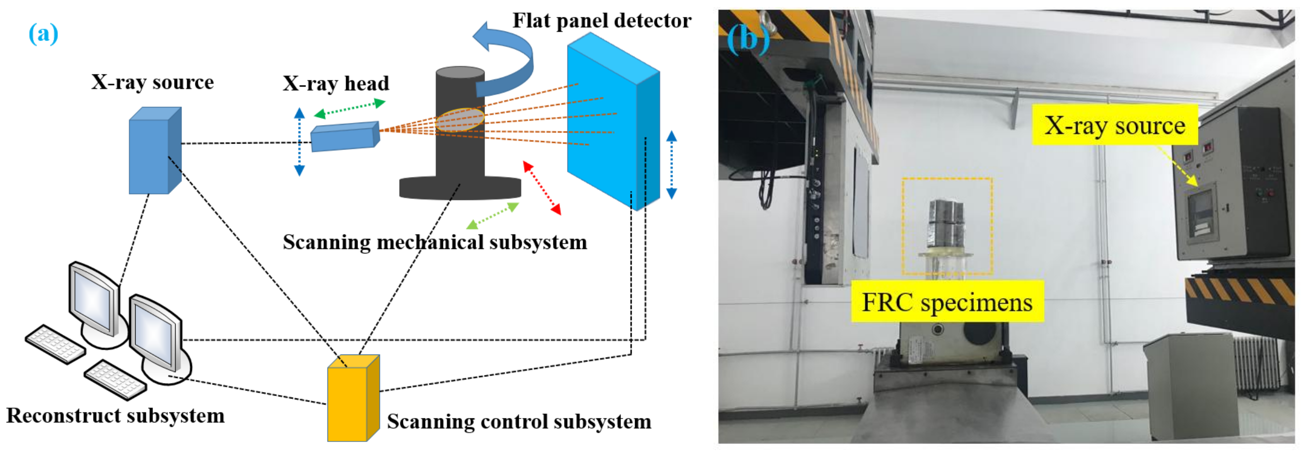

Fig. 5 Industrial CT non-destructive testing system for microstructure investigations: (a) schematic diagram of CT; and (b) photo of CT equipment

2.5 SEM-EDS measurements

A Zeiss Evo 18 scanning electron microscopy coupled with energy dispersive X-ray spectroscopy (SEM-EDS, Berlin, Germany), as shown in Fig. 6, was used to study the microstructural properties of

FRC samples. Samples were taken from the broken sample subjected to different loading rates in form of small pieces/powder. The dried and gilded FRC samples should be prepared for obtaining a true and clear observation during the SEM-EDS measurements. The hydration was terminated by anhydrous ethanol. Note that EDS analysis provides elemental and chemical analysis of a broken FRC sample. The basic parameter was listed as follows: resolution is 3 nm; acceleration voltage is 20 kV; magnification is 5-1000,000 and primary energy is 20 keV. The tested FRC samples for SEM measurements were coated with a sputter coater for at least 20 minutes. Then, the tested FRC samples were placed in the vacuum chamber for more than 30 minutes [61].

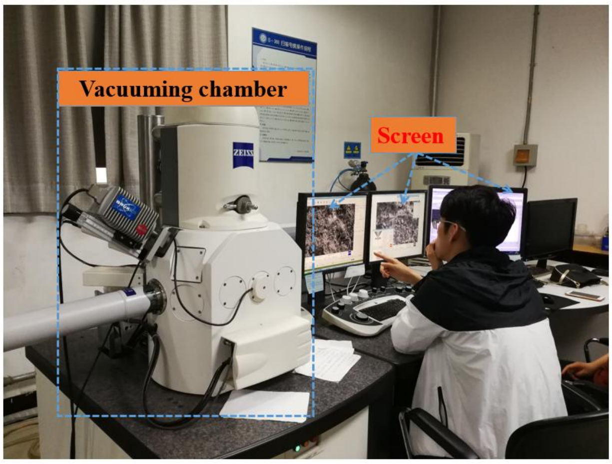

Fig. 6 Photo of ZEISS EVO18 SEM-EDS equipment used

3. Results and discussion

3.1 Effect of fiber type and content on strength development of composites

The relations between UCS and fiber reinforcement of FRC samples were shown in Fig. 7(a). One can observe that, for a fiber content of 0.4 wt.%, 0.8 wt.% and 1.2 wt.% in the matrix, the corresponding average UCS values of glass FRC samples are 20.6 MPa, 19.7 MPa and 16.6 MPa, respectively. For the same fiber contents, the corresponding average UCS values for PP FRC and PAN FRC samples are 21.6 and 18.6 MPa, 20.8 and 19.3 MPa, 17.7 and 11.7 MPa, respectively. Note that the average UCS value of non-fiber-reinforced concrete (NFRC) is 15.6 MPa. It can be interpreted from strength results that the UCS values of all FRC samples increased first and then decreased as the fiber content increased. This is because fibers could effectively limit the crack growth and increase their UCS values during the whole loading process. Certainly, with the increasing fiber content in the matrix, the blended fibers give rise to the development of new bonds in FRC. This unfavorably affects the strength behavior of FRC and cause a slight decrease in its strength when the amount of fiber reaches an optimum value in the mix. Besides, relatively lower strengths also reflect as a result of the unsaturated cement hydration of the matrix. This process can be well explained by the water absorption of fiber and/or the accumulation of water around fiber, leading an unequal distribution of water in FRC. The degree of water retention would be expected to rely on the hydration products formed in the matrix, depending on the type and content of fiber used. Researchers [62-64] have noticed that drainage of water can positively contribute to cement hydration, and accordingly a higher strength development in FRC. To reduce water absorption capacity in fibers and improve fiber-matrix bond interaction, different procedures have been proposed based on applying chemical and physical treatments of both matrix and fiber [65]. The ultimate aim is to reduce porosity in the transition zone and hence boost the fiber-matrix composites. It should be mentioned that the weak bonds established between fibers and cementitious matrices can decline the fiber strengthening effect on cement-fiber matrix composites.

The addition of fiber types also affects the compressive strength of FRC, depending on the interfacial transition zone of cement-fiber-matrix composites. Stress transfer from the matrix to the fiber resulting from frictional slip of fibers at the interface may affect strength properties and geometry of both matrix and fiber. Compared to glass and PAN fibers, which creates a weak bond within FRC as a result of the flocculation or clumping effect, PP fibers provide a strong bridge (i.e., high bonding quality) within the matrix, leading higher strengths. The void filling effect of PP fibers and their good distribution in the matrix also fully affects the strength gain of FRC, reducing water absorption of fiber. A well-established bonding quality between PP and matrix is higher than that of glass and PAN fibers (see SEM results), which effectively fills the gaps within the matrix, and hence increases their strengths and decreases their water absorptions. These results are well proven with the ones present in the literature [66, 67].

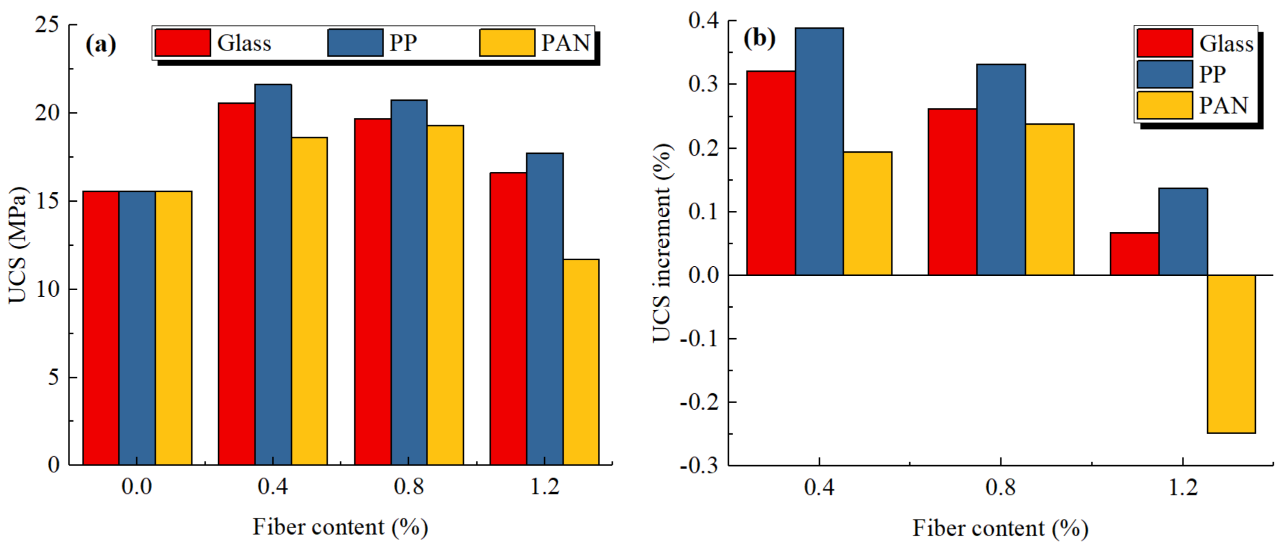

Fig. 7 Bar charts between compressive strength and fiber content: a) UCS; and b) UCS increment

To investigate the effect of fiber type and content on UCS value of FRC samples, the UCS increment ratio was calculated according to equation (1), which was defined as follows:

$$f_{UCS} = \frac{(UCS_{FRC} - UCS_{NFRC})}{UCS_{NFRC}} \times 100\% \quad (1)$$

where f_{UCS} is the UCS increment ratio, UCS_{FRC} and UCS_{NFRC} are the compressive strength value of FRC and non-fiber-reinforced concrete (NFRC) samples, receptively.

Fig. 7(b) shows the relation between UCS increment ratio and fiber content. It was found that the UCS increment ratios of FRC specimens gradually decreased as the fiber content increased. When the fiber content is 0.4 wt.%, 0.8 wt.%, and 1.2 wt.%, the UCS increment ratios of glass FRC samples are 32.1%, 26.2% and 6.6%, respectively. In addition, the UCS increment ratios corresponding to both PP FRC and PAN FRC samples are 38.9% and 19.4%, 33.2% and 23.8%, 13.7% and -24.8%, respectively. It was also found that when the fiber content was less than 0.8 wt.%, the UCS increment ratio of three kinds FRC samples was larger than 19%, and the maximum is close to 39%. Likewise, when the fiber content exceeds 0.8 wt.%, the UCS increment ratio reduces steeply. The UCS increment ratio of PAN FRC showed a negative value, which was lower than NFRC samples.

3.2 Effect of fiber type and content on stress-strain behavior of composites

Fig. 8 shows the stress-strain curves of FRC and NFRC samples. One can observe in this figure that increasing on FRC strength makes stress-strain curve less stretched and increases the peak stress.

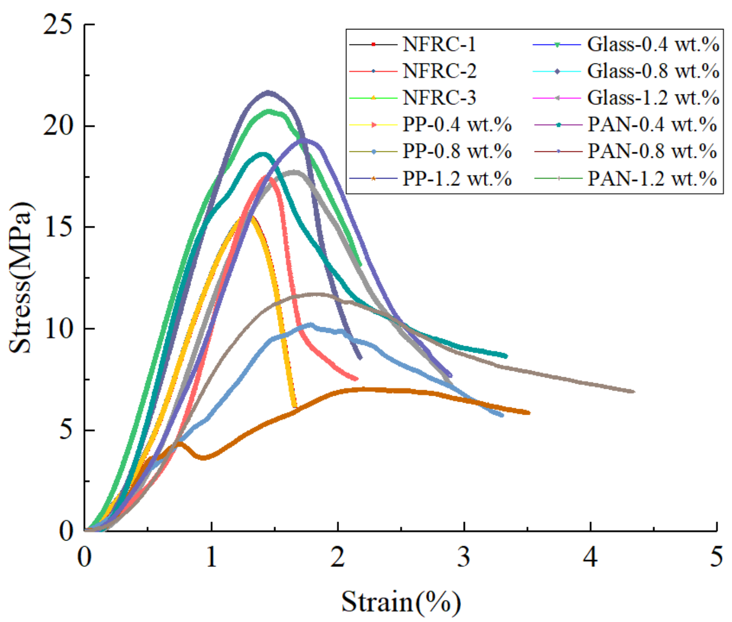

Fig. 8 Relations between strain and stress of NFRC and FRC specimens

In addition, in a given volume, higher the volume of fibers, higher will be the strength and toughness of FRC. However, addition of higher volume of fibers leads to problems such as bundling, balling and reduction in workability, strength and toughness. The strengths of NFRC samples dropped sharply after the peak strain, while UCS of FRC ones decreased gradually after the peak strain. This is because the internal fibers of FRC samples resist the propagation of cracks during the whole loading process. Even after the peak strength, the bridging effect of fiber could still effectively prevent the crack formation from propagating again. FRC showed good ductility characteristics. However, the brittle properties of NFRC samples caused them to quickly lose their loading capacity after the peak strain.

The mechanism of fiber strengthening in compression can be explained as follows. If the frictional forces between loading platens and the surfaces of the compressive samples are minimized, then failure of FRC by lateral expansion under uniaxial compression is possible. Indeed, cracking of FRC samples starts to occur before reaching the end load, as witnessed by a decrease in gradient of the rising portion of the stress-strain curve. After reaching the end load, the internal cracks start to interconnect, hence reducing the overall stiffness of FRC. The increases in toughness count on the volume fraction of fibers and on effectiveness of fibers bridging tensile cracks. Randomly distributed fibers can be less effective, while fibers parallel to the loading direction can five lower strengths due to buckling of fibers [68, 69].

Generally, the stress-strain curves of PP FRC samples indicate higher fracture toughness than those for glass and PAN fibers, mainly owing to the size of fibers used, the shape of samples and the direction of casting. The possible reasons why the strength gain of FRC is increased by the addition of PP fibers, are that fibers tend to confine sample's lateral expansion thereby reducing the propagation of cracking, and that the protruding fibers at the loading surfaces of sample tend to increase the frictional forces between sample and the loading platens of the machine.

3.3 Effect of fiber type and content on peak strain of composites

A clear relation between peak strain and fiber content of glass, PP and PAN FRC samples was shown in Fig. 9. The linear fitting method was used to better explore the quantitative relationship between fiber content and peak strain of FRC samples. It was found that the multiple correlation coefficient of linear fitting is 0.9363, 0.9542 and 0.9552. In addition, the slope of peak strain of glass, PP and PAN FRC samples was 0.263, 0.755 and 0.486, respectively. In other words, adding the same amount of fiber to the prepared FRC mix to improve energy absorption and apparent ductility, PP fiber is more effective than other two fibers (i.e., glass and PAN) in increasing peak strain. The previous results also confirmed the higher efficiency of PP fibers in increasing the ductility and energy absorption when compared to those of glass and PAN fibers [70].

It is well-known that high strength concretes are considered to be a relatively brittle material. To improve its ductility, and ability to absorb energy prior to failure, fibers are added to the concrete mix. The ductility of a material is shown through the energy absorbed by a material until a complete failure takes place. This energy is measured by the area under the stress-strain curve. Commonly, the increase in ductility and energy absorption is proportional to the increase in the fiber content. This is because the inclusion of fibers significantly increases the ultimate strength, stiffness and ductility of FRC since fiber controls crack growth due to plastic shrinkage and drying shrinkage, thereby reducing the permeability of FRC. When fibers are present, the cracks cannot extend without stretching and debonding fibers. As a result, substantial additional energy is required before complete fracture of FRC occurs. Hence, increase in the toughness is a significant improvement resulting from the addition of fibers. The key parameters influencing toughness of FRC are the type, volume percentage, aspect ratio, nature of deformation, and orientation of fiber itself [29, 30, 34].

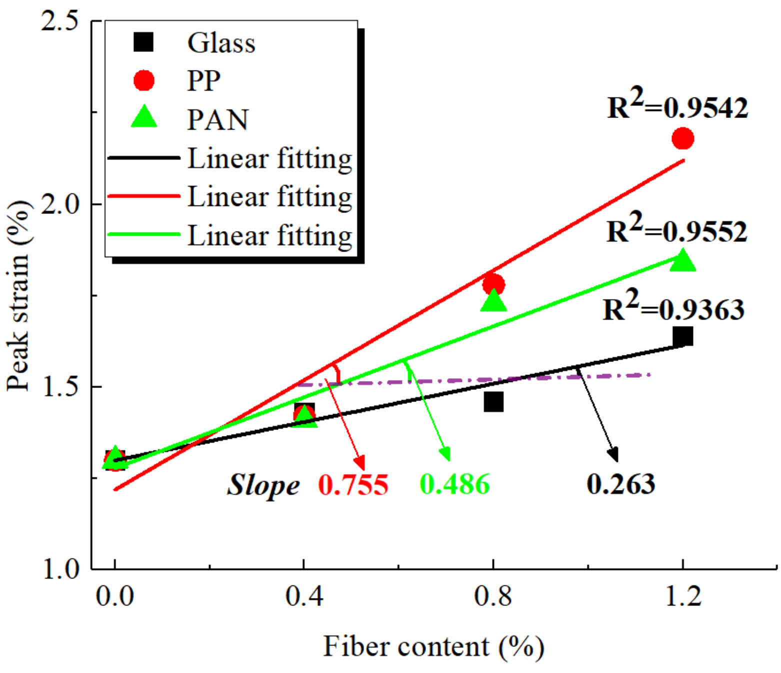

Fig. 9 Relationship between peak strain and fiber content for all samples

One can express from Fig. 9 that the peak strain vales increases with increasing fiber content in FRC. This can be explained by the increased cohesive strength of the matrix by fiber and cement hydration. All curves clearly reveal that the initial stiffness of FRC samples, regardless of fiber type and content, was slightly reduced by adding fibers. Seemingly, the addition of fibers hindered cementing bonds and produced more pores and micro cracks within the matrix. However, fiber reinforcement had a distinct influence on strength after an axial strain of 1.5%. This was thus obvious for PP FRC samples where the corresponding strength gain was the highest among others. Besides, the cementing bonds are mobilized at small strains which describe the more ductile behavior of FRC for a given matrix recipe. When the cracks develop in the matrix (including the strain hardening/softening process), the cohesion will be lost completely along the crack surfaces. When the cohesion is very small, e.g., on very brittle interfaces, it can be shown that the only parameter which matters is the facture energy. But, when the cohesion is very large and comparable with the dimensions of the FRC structure, results can be strongly affected by the other parameters, such as the peak stress, the ultimate strength and stiffness.

3.4 Assessment of computed tomography scan analysis

Fig. 10 shows the 2D cross-sectional computed tomography (CT) scan images of NFRC samples. One can comment that well-defined failure planes appear around the section of FRC without fibers. Because of the increased ductility, the cracks and pores became more obvious when Z is increased from 35 to 65 mm. It is also clear that cracks within the matrix develops and expands more easily in the side wall of samples instead of a middle part of the matrix. Without fiber, samples are subjected to external stresses as well as confinements and load surcharges exerted from the adjacent stope.

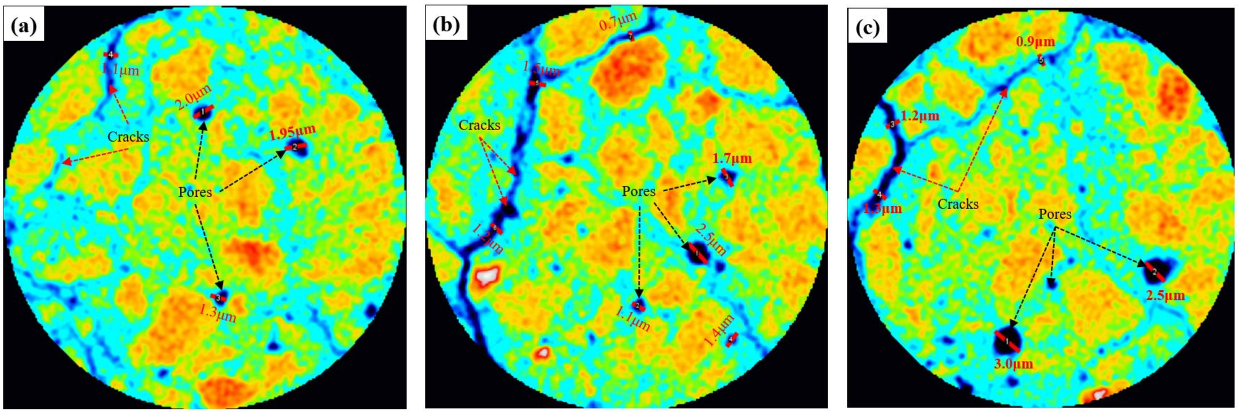

Fig. 10 2D CT images of NFRC samples: a) Z = 35 mm; b) Z = 50 mm; and c) Z = 65 mm

In addition, dark blue represents cracks and pores and orange yellow represents gravels in these figures. Among them, the shape of pores was mainly dark blue circles. The size dimensions of these pores were between 0.4μm and 3.0μm. Besides, these cracks mainly existed at the edges of NFRC in Fig. 10(a), and these cracks were not well connected to each other. There is not any binding and/or connecting element within the matrix, such as fiber reinforcement. However, the developed cracks had a clear connection together, as shown in Fig. 10(b) and Fig. 10(c).

Figs. 11-13 clearly demonstrate the 2D CT images of glass FRC, PP FRC and PAN FRC samples, respectively. It was observed from Fig. 11 that the crack numbers of glass FRC samples within the different cross section were more than NFRC ones. Two nearly parallel cracks appeared on the cross sections when the fiber content is 0.4 wt.%. The crack width was between 0.7-1.8μm. When the fiber content is 0.8 wt.%, only one obvious crack appeared on the sections. The width of this crack was significantly larger than that of those FRC samples with a fiber content of 0.4 wt.%. The widest crack in the matrix was 2.39μm. However, the cracks within FRC did not cut off the gravels but expanded and penetrated along the gravels. In a given volume, shorter the length of fiber, closer will be the spacing of fibers and will be as near as possible to micro-cracks. These fibers may contribute to delay in formation cracks but may be pulled out after micro-cracks transformed into macro-cracks. Then long length fibers bridge crack and improves post-crack deformations of FRC, as the length of fiber increases resistance to post-crack deformation increases. Accordingly, an ideal blending of fibers may enhance FRC's strength and improves its overall deformations.

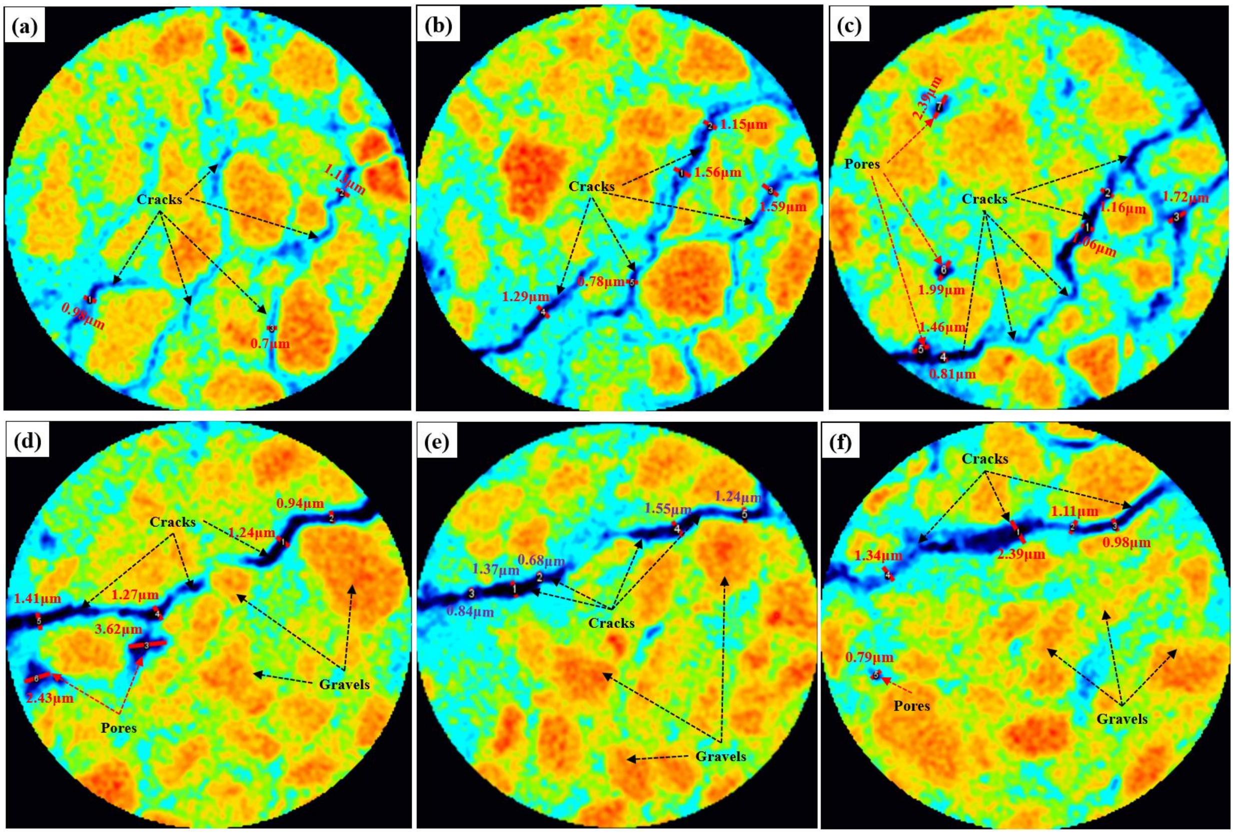

Fig. 11 2D CT images of glass FRC samples: a) G-0.4, Z = 35 mm; b) G-0.4, Z = 50 mm; c) G-0.4, Z = 65 mm; d) G-0.8, Z = 35 mm; e) G-0.8, Z = 50 mm; and f) G-0.8, Z = 65 mm

It should be also kept in mind that the micro-structure of FRC plays a significant role in its macro properties for a given matrix recipe. Compared with NFRC samples, the addition of fibers to the mix makes FRC a complicated microstructure which should be characterized meticulously in the laboratory environment. As a multi-interface composite material, the behavior of FRC depends largely on quality and properties of the interface transition zone between fiber and cementitious matrix. The good bonding quality of fiber-matrix will improve the strength characteristics and reduce the water absorption of FRC. Fig. 12 shows that the number of cracks in the cross section of PP FRC samples was large, but the distribution was fairly dispersed. The inner corresponding crack width was less than 1.2μm when the fiber content is 0.4 wt.%. Only some cracks at the boundary were larger than 1.2μm.

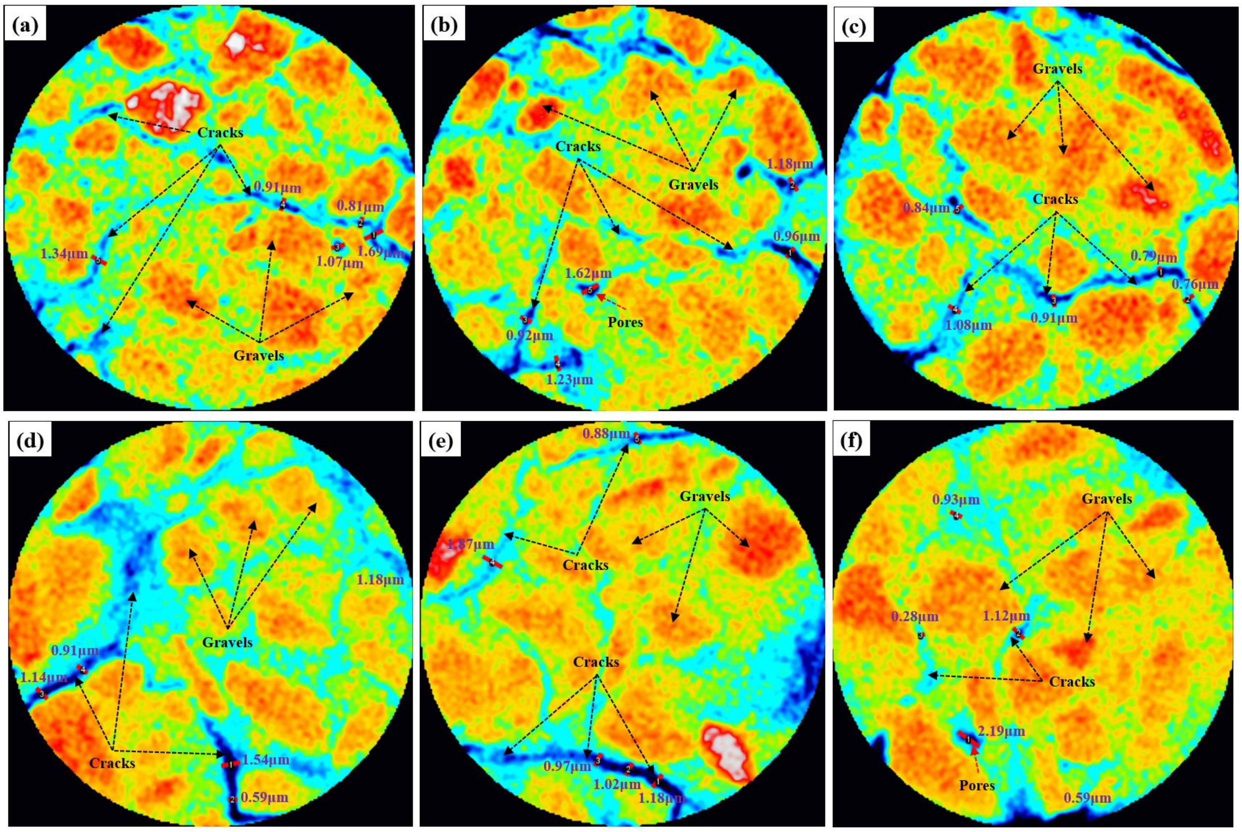

Fig. 12 2D CT images of PP FRC samples: a) PP-0.4, Z = 35 mm; b) PP-0.4, Z = 50 mm; c) PP-0.4, Z = 65 mm; d) PP-0.8, Z = 35 mm; e) PP-0.8, Z = 50 mm; and f) PP-0.8, Z = 65 mm

Only one main unconnected crack was found in Fig. 13(a-c), most of the cracks had a small width (less than 1.11 μm), but a long length when the fiber content was 0.4 wt.%. Besides, the location of cracks nearly in the middle of each section. However, the distribution of cracks in Fig. 13(d-f) were relatively scattered. Besides, most of the crack width were less than 0.92μm.

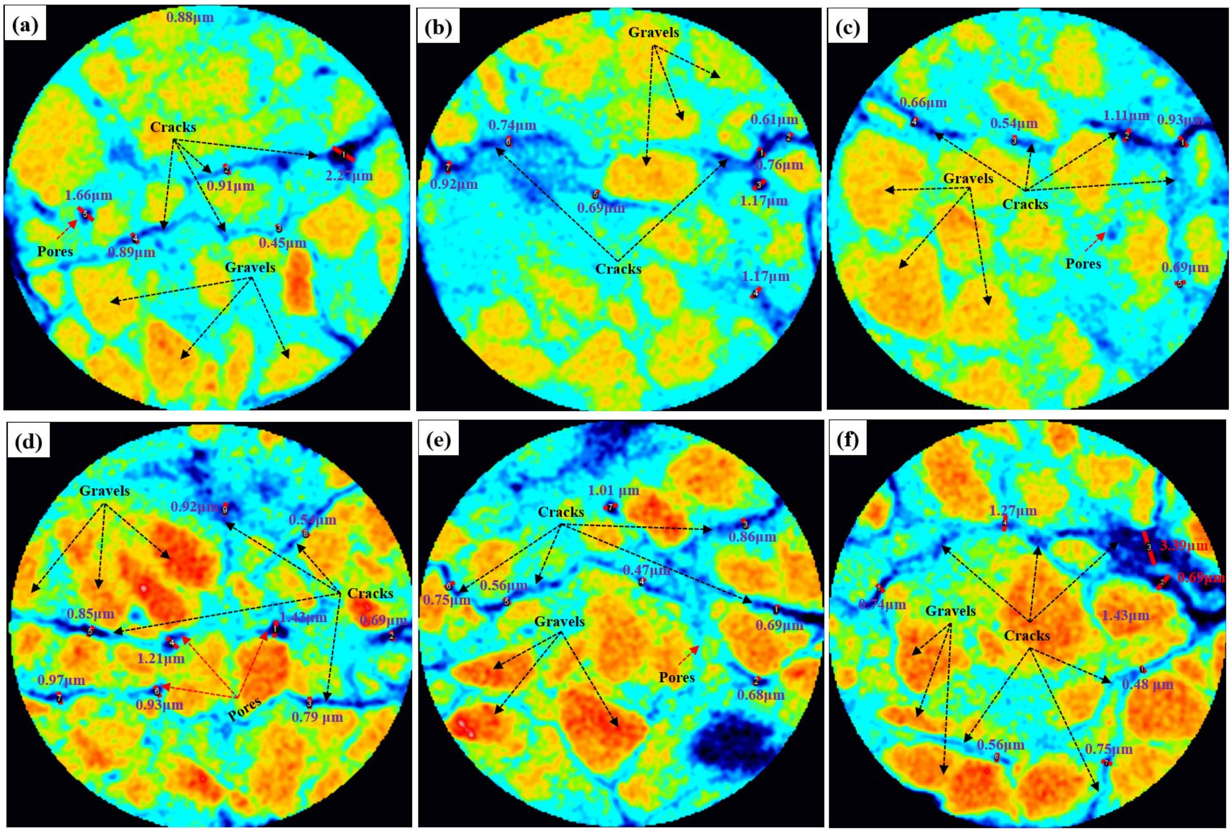

Fig. 13 2D CT images of PAN FRC samples: a) PAN = 0.4, Z = 35 mm; b) PAN = 0.4, Z = 50 mm; c) PAN = 0.4, Z = 65 mm; d) PAN = 0.8, Z = 35 mm; e) PAN = 0.8, Z = 50 mm; and f) PAN = 0.8, Z = 65 mm

As a result, one can say that the cross-sectional images obtained from computed tomography (CT) scan test explain the ductile behavior as the limit to crack propagation and extension by the tensile strength of mobilized fiber in the FRC matrix for a given recipe.

3.5 Assessment of SEM-EDS measurements

To better study the microstructure of different types of FRC samples, SEM-EDS measurements were used to comprehensively analyze the surface internal structure of the prepared FRC samples. Figs. 14 and 15 illustrate both SEM and EDS analyses of glass, PP and PAN FRC samples at a fiber content of 0.4 wt.%, 0.8 wt.% and 1.2 wt.%. One can visibly observe from Fig. 14 that the failure mode of fiber reinforced concrete samples exhibited ductile behavior, remaining a full integrity.

Although the CT scan results could also analyze microscopic parameters such as pores and crack sizes, SEM-EDS can obtain more detail information, such as the hydrated elemental composition and fiber distribution information. It was observed from Fig. 14 that many ettringites and calcium silicate hydrates (C-S-H) exist in the glass FRC matrix. Cracks and pores distributed in the surface were notable as well. Besides, it was found that fibers and hydration products (HP) were in close contact, which increase the friction between fiber and HP. It can limit crack growth under external load and improved the strength of glass FRC. Fibers were also in close contact with HP in Fig. 14(d) and Fig. 14(g) when the fiber content was 0.4 wt.%.

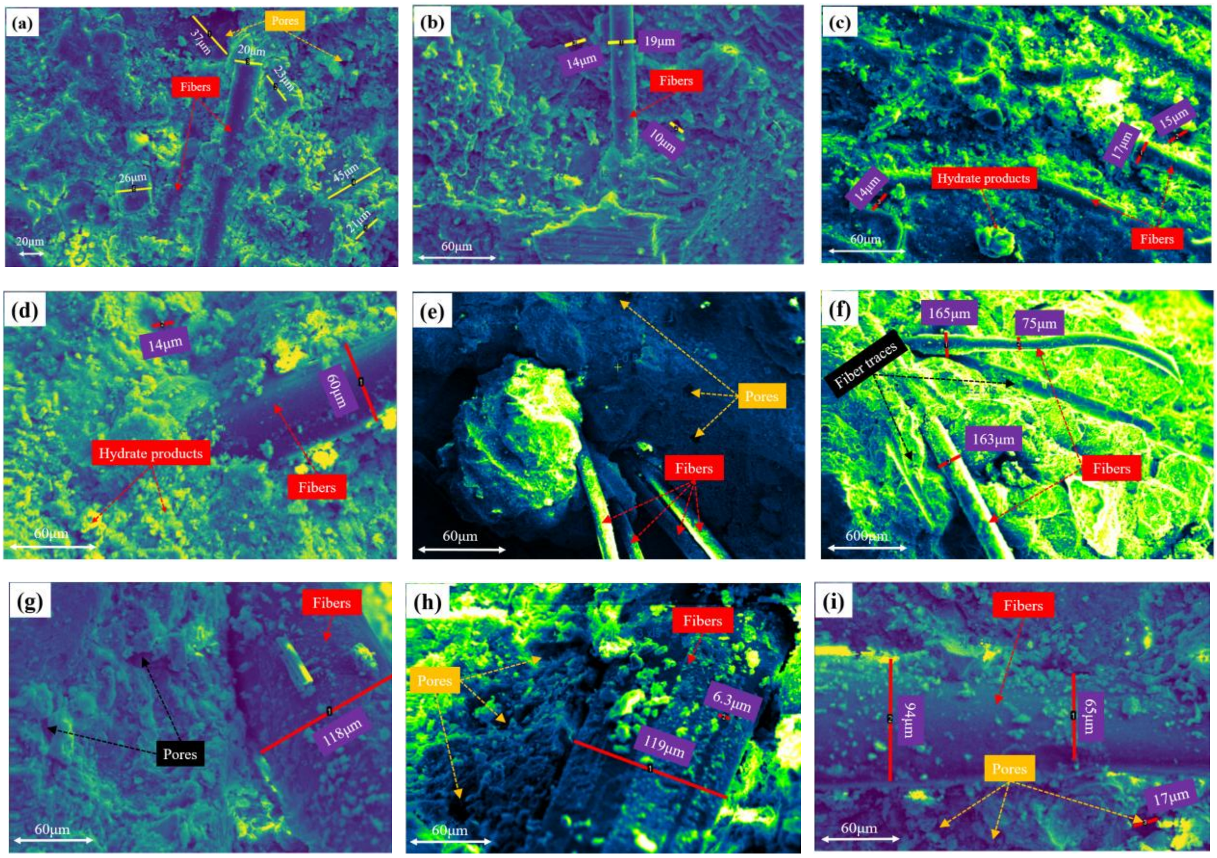

Fig. 14 SEM micrographs of FRC samples: a) G-0.4; b) G-0.8; c) G-1.2; d) PP-0.4; e) PP-0.8; f) PP-1.2; g) PAN-0.4; h) PAN-0.8; and i) PAN-1.2

Several bundles of parallel fibers were distributed in Fig. 14(e) because of mixing process. Fibers were pulled out because of external loading. In addition, the fiber diameter also changed, and the same fiber has different diameters, with a maximum diameter of 165μm and a minimum diameter of 75μm. This is due to the tensile change of the fiber caused by the traction of crack propagation under external loads. The diameters of PP and PAN were 18-48 and 10-35μm, respectively. The fiber diameters in this SEM images were larger. For example, the fiber diameters in Fig. 14(h) and Fig. 14(i) were 119μm and 94μm, respectively. This was due to the expansion and deformation of the fiber caused by the combined action of water soaking and hydration reaction exotherm. As a result, one can interpret from the analysis of SEM micrographs, the crack formations and micro-mechanical properties of FRC are closely related not only with fiber distribution but also with fiber orientation.

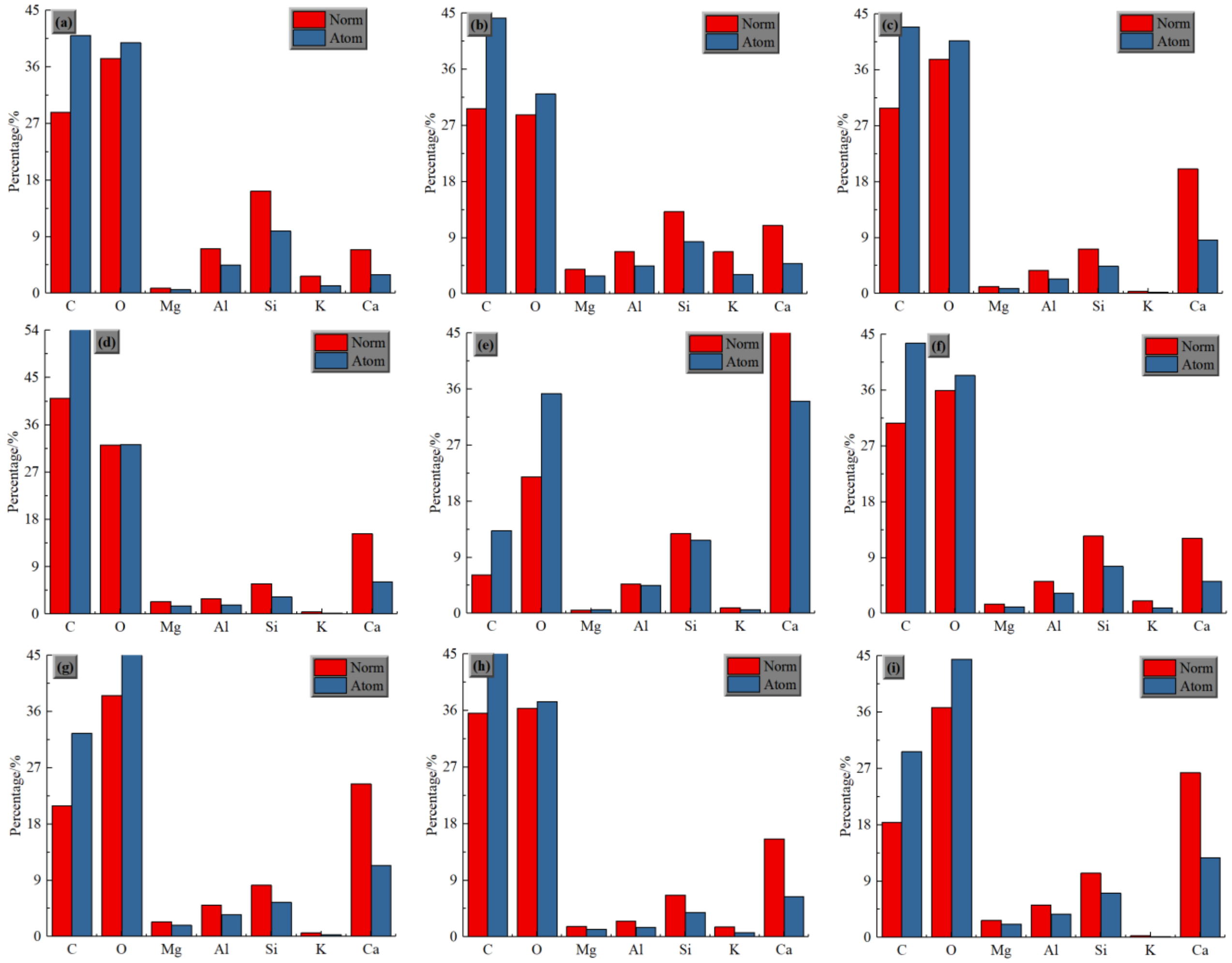

Fig. 15 Analysis of the EDS values of FRC samples: a) G-0.4; b) G-0.8; c) G-1.2; d) PP-0.4; e) PP-0.8; f) PP-1.2; g) PAN-0.4; h) PAN-0.8; and i) PAN-1.2

The elements in tested samples were mainly include C, O, Mg, Al, Si, K and Ca according to Fig. 15. The presence of element such Si, Ca and Al affected the strength of FRC. Production of C-S-H and other products of hydration in the presence of such elements improves [71].

4. Conclusions

In this study, some UCS, CT scan and SEM-EDS measurements were undertaken on FRC samples considering the fiber type and content effects. The mechanical and microstructural properties of FRC samples were evaluated as a function of fiber type (e.g., glass, PP and PAN fibers) and fiber content (0 wt.%, 0.4 wt.%, 0.8 wt.% and 1.2 wt.%). A total of 30 FRC samples were prepared and subjected to UCS, CT and SEM-EDS tests. From the performed tests, the following conclusions can be drawn:

- UCS values of all FRC samples increase first and then decrease as the fiber content increased as a result of the enhanced fiber volume ratio. The UCS increment ratio within FRC samples gradually decreased as the fiber content increased.

- The fraction of fiber reinforcement is forceful in determining the overall mechanical properties of cementitious materials such as FRC. For a given concrete recipe, a higher fiber volume fraction typically results in better mechanical properties of FRC.
- The increased amount of fibers increases the interaction of fibers with each other during mixing, leading to problems such as bundling and balling, and decreases the FRC's workability first and then mechanical strength performance.
- Introducing fibers in the FRC mix enhances the stress-strain characteristics and improves the post peak behavior; this is reflected by an increase in ductility and toughness of the resulting FRC.
- PP fiber was more effective than both glass and PAN fibers in increasing peak strain. The peak strain increases linearly with increasing fiber content.
- Reinforcement plays a key role on UCS performance of FRC samples. Fiber reinforced concretes exhibited more plasticity, showing the ability to sustain stress levels in peak stress at much higher strain levels than non-reinforced samples.

The preliminary series of experimental tests given in this study have identified some trends in the quality and behavior of FRC materials. Additional tests are underway to evaluate the effect of different reinforcement measures and sample sizes in the laboratory. Field trials are also underway in a mine to measure the effects of artificial pillar reinforcement. As a result, developing an understanding of the influence of reinforcement on strength and stability of artificial pillars will offer engineers with a further tool which can be used to deal with unfavorable ground conditions.

Declaration of Competing Interest

The authors declare that the work described has not been published before; that it is not under consideration for publication anywhere else; that its publication has been approved by all co-authors; that there is no conflict of interest regarding the publication of this article.

Acknowledgments

This work was financially supported by the National Natural Science Foundation of China (Grant numbers 51804017 and 51974012), the China Postdoctoral Science Foundation (Grant number 2018M631341), the Open Fund of Key Laboratory of Ministry of Education for Efficient Mining and Safety of Metal Mines (Grant number USTBMSLAB201804) and the Fundamental Research Funds for Central Universities (Grant number FRF-TP-17-075A1). The authors want to sincerely acknowledge the technical assistance provided in the laboratory.

References

[1] Skrzypkowski, K., 2019. The influence of room and pillar method geometry on the deposit utilization rate and rock bolt load. Energies, 12, 4770.

[2] Luo, Y., 2015. Room-and-pillar panel design. Mining Engineering, 67(7), 105-110.

[3] Xia, K.Z., Chen, C.X., Deng, Y.Y., Xiao, G.F., Zheng, Y., Liu, X.M., Fu, H., Son, X.G., Chen, L.L., 2018. In situ monitoring and analysis of the mining-induced deep ground movement in a metal mine. International Journal of Rock Mechanics and Mining Sciences, 109, 32-51.

[4] Cao, S., Yilmaz, E., Song, W., Yilmaz, E., Xue, G., 2019. Loading rate effect on uniaxial compressive strength behavior and acoustic emission properties of cemented tailings backfill. Construction and Building Materials, 213, 313-324.

[5] Jessu, K.V., Spearing, A.J.S., Sharifzadeh, M., 2018. Laboratory and numerical investigation on strength performance of inclined pillars. Energies, 11, 3229.

[6] Martin, C.D., Kaiser, P.K., Christiansson, R., 2003. Stress, instability and design of underground excavations. International Journal of Rock Mechanics and Mining Sciences, 40(7-8), 1027-1040.

[7] Malli, T., Yetkin, M.E., Ozfirat, M.K., Kahraman, B., 2017. Numerical analysis of underground space and pillar design in metalliferous mine. Journal of African Earth Science, 134, 365-372.

[8] Yu, Y., Chen, S.-E., Deng, K.-Z., Fan, H.-D., 2017. Long-term stability evaluation and pillar design criterion for room-and-pillar mines. Energies, 10, 1644.

[9] Esterhuizen, G.S., Dolinar, D.R., Ellenberger, G.L., 2011. Pillar strength in underground stone mines in the United States. International Journal of Rock Mechanics and Mining Sciences, 48, 42-50.

[10] Tesarik, D.R., Seymour, J.B., Yanske, T.R., 2009. Long-term stability of a backfilled room and pillar test section at the Buick Mine, Missouri, USA. International Journal of Rock Mechanics and Mining Sciences, 46, 1182-1196.

[11] Renani, H.R., Martin, C.D., 2018. Modeling the progressive failure of hard rock pillars. Tunneling and Underground Space Technology, 74, 71-81.

[12] Yilmaz, E., Belem, T., Benzaazoua, M. Study of physico-chemical and mechanical characteristics of consolidated and unconsolidated cemented paste backfills. Miner. Resour. Manag., 2013, 29(1), 81-100.

[13] Cao, R.H., Cao, P., Lin, H., 2016. Support technology of deep roadway under high stress and its application. International Journal of Mining Science and Technology, 26(5), 787-793.

[14] Xue, G., Yilmaz, E., Song, W., Cao, S., 2018. Compressive strength characteristics of cemented tailings backfill with alkali-activated slag. Applied Sciences, 8(9), 1537.

[15] Mark, C., 2016. Science of empirical design in mining ground control. International Journal of Mining Science and Technology, 26(3), 461-470.

[16] Li, Y.H., Li, K.M., Feng, X.T., Cai, M., 2018. Development and evaluation of artificial expandable pillars for hard rock mining. International Journal of Rock Mechanics and Mining Sciences, 110, 68-75.

[17] Waclawik, P., Snuparek, R., Kukutsch, R., 2017. Rock bolting at the room and pillar method at great depth. Procedia Engineering, 191, 575-582.

[18] Yu, Y., Deng, K.Z., Luo, Y., Chen, S.E., Zhuang, H.F., 2018. An improved method for long-term stability evaluation of strip mining and pillar design. International Journal of Rock Mechanics and Mining Sciences, 105, 98-109.

[19] Sun, Q., Zhang, J.X., Zhou, N., 2018. Study and discussion of short-strip coal pillar recovery with cemented paste backfill. International Journal of Rock Mechanics and Mining Sciences, 104, 147-155.

[20] Hauquin, T., Deck, O., Gunzburger, Y., 2016. Average vertical stress on irregular elastic pillars estimated by a function of the relative extraction ratio. Int. Journal of Rock Mechanics and Mining Sciences, 83, 122-134.

[21] Ghasemi, E., Ataei, M., Shahriar, K., 2014. An intelligent approach to predict pillar sizing in designing room and pillar coal mines. International Journal of Rock Mechanics and Mining Sciences, 65, 86-95.

[22] Shi, J.W., Cao, W.H., Wu, Z.S., 2019. Effect of adhesive properties on the bond behavior of externally bonded FRP-to-concrete joints. Composites Part B: Engineering, 177, 107365.

[23] Wang, P., Gao, N., Ji, K., Stewart, L., Arson, C., 2019. DEM analysis on the role of aggregates on concrete strength. Computers and Geotechnics, 2019, https://doi.org/10.1016/j.compgeo.2019.103290.

[24] Arabzadeh, A., Notani, M.A., Zadeh, A.K., Nahvi, A., Sassani, A., Ceylan, H., 2019. Electrically conductive asphalt concrete: An alternative for automating the winter maintenance operations of transportation infrastructure. Composites Part B: Engineering, 173, 106985.

[25] Mesgari, S., Akbarnezhad, A., Xiao, J.Z., 2020. Recycled geopolymer aggregates as coarse aggregates for Portland cement concrete and geopolymer concrete: Effect on mechanical properties. Construction and Building Materials, 236, 117571.

[26] Qing, L.B., Cheng, Y.H., Fan, X.Q., Mu, R., Ding, S.Q., 2020. An arc bending notched specimen for determining the mechanical and fracture parameters of concrete based on the FET. Engineering Fracture Mechanics, 220, 106639.

[27] Ren, D.R., Liu, B.G., Sun, J.L., Song, Y., Lin, Z.J., Liu, B.K., 2019. Interevent acoustic emission character of three-point-bending tests on concrete beams by the nearest neighbor distance. Construction and Building Materials, 224, 359-371.

[28] Fu, C.Q., Ye, H.L., Wang, K.J., Zhu, K.Q., He, C.Y., 2019. Evolution of mechanical properties of steel fiber-reinforced rubberized concrete (FR-RC). Int. Journal of Composites Part B: Engineering, 160, 158-166.

[29] Folino, P., Ripani, M., Xargay, H., Rocca, N., 2020. Comprehensive analysis of fiber reinforced concrete beams with conventional reinforcement. Engineering Structures, 202, 109862.

[30] Carlesso, D.M., Fuente, A.D.L., Cavalaro, S.H.P., 2019. Fatigue of cracked high-performance fiber reinforced concrete subjected to bending. Construction and Building Materials, 220, 444-455.

[31] Kazmi, S.M., Munir, M.J., Wu, Y., Patnaikuni, I., Zhou, Y., Xing, F., 2019. Axial stress-strain behavior of macro-synthetic fiber reinforced recycled aggregate concrete. Cement & Concrete Composites, 97, 341-356.

[32] Signorini, C., Sola, A., Malchiodi, B., Nobili, A., Gatto, A., 2019. Failure mechanism of silica coated polypropylene fibres for fibre reinforced concrete (FRC). Construction and Building Materials, 228, 117549.

[33] Chen, M., Zhong, H., Zhang, M.Z., 2020. Flexural fatigue behaviour of recycled tyre polymer fibre reinforced concrete. Cement and Concrete Composites, 105, 103441.

[34] Le, L.A., Nguyen, G.D., Bui, H.H., Sheikh, A.H., Kotousov, A., 2019. Incorporation of micro-cracking and fibre bridging mechanisms in constitutive modelling of fibre reinforced concrete. Journal of the Mechanics and Physics of Solids, 133, 103732.

[35] Usman, M., Farooq, S.H., Umair, M., Hanif, A., 2019. Axial compressive behavior of confined steel fiber reinforced high strength concrete. Construction and Building Materials, 228, 117043.

[36] Liu, J.L., Jia, Y.M., Wang, J., 2019. Calculation of chloride ion diffusion in glass and polypropylene fiber-reinforced concrete. Construction and Building Materials, 215, 875-885.

[37] Liu, F.Y., Ding, W.Q., Qiao, Y.F., 2019. Experimental investigation on the flexural behavior of hybrid steel-PVA fiber reinforced concrete containing fly ash and slag powder. Construction and Building Materials, 228, 116706.

[38] Afroughsabet, V., Geng, G.Q., Lin, A., Biozi, L., Ostertag, C.P., Monteiro, P.J.M., 2019. The influence of expansive cement on the mechanical, physical, and microstructural properties of hybrid-fiber-reinforced concrete. Cement and Concrete Composites, 96, 21-32.

[39] Kou, M.M., Liu, X.R., Tang, S.D., Wang, Y.T., 2019. 3-D X-ray computed tomography on failure characteristics of rock-like materials under coupled hydro-mechanical loading. Theoretical and Applied Fracture Mechanics, 104, 102396.

[40] Yang, S.Q., Yin, P.F., Huang, Y.H., Cheng, J.L., 2019. Strength, deformability and X-ray micro-CT observations of transversely isotropic composite rock under different confining pressures. Engineering Fracture Mechanics, 214, 1-20.

[41] Xue, G.L., Yilmaz, E., Song, W.D., Cao, S., 2019. Analysis of internal structure behavior of fiber reinforced cement-tailings matrix composites through X-ray computed tomography. Composites Part B: Engineering, 175, 107091.

[42] Cao, S., Xue, G., Yilmaz, E., 2019. Flexural behavior of fiber reinforced cemented tailings backfill under three-point bending. IEEE Access, 7(1), 139317-139328.

[43] Koohestani, B., Darban, A.K., Mokhtari, P., Yilmaz, E., Darezereshki, E., 2019. Comparison of different natural fibers treatments-A literature review. International Journal of Environmental Science and Technology, 16(1), 629-642.

[44] Xue, G., Yilmaz, E., Song, W., Yilmaz, E., 2019. Influence of fiber reinforcement on mechanical behavior and microstructural properties of cemented tailings backfill. Construction and Building Materials, 213, 275-285.

[45] Jiang, H., Qi, Z., Yilmaz, E., Han, J., Qiu, J., Dong, C., 2019. Effectiveness of alkali-activated slag as alternative binder on workability and early age compressive strength of cemented paste backfills. Construction and Building Materials, 218, 689-700.

[46] Xue, G., Yilmaz, E., Song, W., Cao, S., 2019. Mechanical, flexural and microstructural properties of cement-tailings matrix composites: Effect of fiber type and dosage. Composites Part B: Engineering, 172, 131-142.

[47] Jiang, H., Yi, H., Yilmaz, E., Liu, S., Qiu, J., 2020. Ultrasonic evaluation of strength properties of cemented paste backfill: Effects of mineral admixture and curing temperature. Ultrasonics, 100, 105983.

[48] Cao, S., Yilmaz, E., Song, W., 2018. Dynamic response of cement-tailings matrix composites under SHPB compression load. Construction and Building Materials, 186, 892-903.

[49] Xue, G., Yilmaz, E., Song, W., Cao, S., 2020. Fiber length effect on strength properties of polypropylene fiber reinforced cemented tailings backfill specimens with different sizes. Construction and Building Materials, 241, 118113.

[50] Cao, S., Yilmaz, E., Xue, G., Song, W., 2019. Assessment of acoustic emission and triaxial mechanical properties of rock-cemented tailings matrix composites. Advances in Materials Science and Engineering, Article 6742392, 12p, https://doi.org/10.1155/2019/6742392.

[51] Jalal, M., Nassir, N., Jalal, H., Arabali, P., 2019. On the strength and pulse velocity of rubberized concrete containing silica fume and zeolite: Prediction using multivariable regression models. Construction and Building Materials, 223, 530-543.

[52] Ríos, J.D., Cifuentes, H., Leiva, C., Seitl, S., 2019. Analysis of the mechanical and fracture behavior of

heated ultra-high-performance fiber-reinforced concrete by X-ray computed tomography. Cement and Concrete Research, 119, 77-88.

[53] Schock, J., Liebl, S., Achterhold, K., Pfeiffer, F., 2016. Obtaining the spacing factor of microporous concrete using high-resolution dual energy X-ray micro CT. Cement and Concrete Research, 89, 200-205.

[54] Wang, Z., Gong, F.Y., Zhang, D.W., Hayashida, H., Ueda, T., 2017. Mesoscale simulation of concrete behavior with non-uniform frost damage with verification by CT imaging. Construction and Building Materials, 157, 203-213.

[55] Henry, M., Darma, I.S., Sugiyama, T., 2014. Analysis of the effect of heating and re-curing on the microstructure of high-strength concrete using X-ray CT. Construction and Building Materials, 67, 37-46.

[56] Zhang, J., Ma, G.D., Ming, R.P., Cui, X.Z., Li, L., Xu, H.N., 2018. Numerical study on seepage flow in pervious concrete based on 3D CT imaging. Construction and Building Materials, 161, 468-478.

[57] Yu, F., Sun, D.Q., Hu, M.J., Wang, J., 2019. Study on the pores characteristics and permeability simulation of pervious concrete based on 2D/3D CT images. Construction and Building Materials, 200, 687-702.

[58] Chung, S.Y., Han, T.S., Kim, S.Y., Kim, J.H.J., Youm, K.S., Lim, J.H., 2016. Evaluation of effect of glass beads on thermal conductivity of insulating concrete using micro CT images and probability functions. Cement and Concrete Composites, 65, 150-162.

[59] Vicente, M., Mínguez, J., González, D., 2019. Computed tomography scanning of the internal microstructure, crack mechanisms, and structural behavior of fiber-reinforced concrete under static and cyclic bending tests. International Journal of Fatigue, 121, 9-19.

[60] Huang, H., Yuan, Y.J., Zhang, W., Hao R.Q., Zeng, J., 2020. Bond properties between GFRP bars and hybrid fiber-reinforced concrete containing three types of artificial fibers. Construction and Building Materials, 250: 118857.

[61] Stelzner, L., Powierza, B., Oesch, T., Dlugosch, R., Weise, F., 2019. Thermally induced moisture transport in high-performance concrete studied by X-ray-CT and H-NMR. Constr. Building Materials, 224, 600-609.

[62] Soe, K., Zhang, Y.X., Zhang, L.C., 2013. Material properties of a new hybrid fibre-reinforced engineered cementitious composites. Construction and Building Materials, 43, 399-407.

[63] Qian, C.X., Stroeven, P., 2000. Development of hybrid polypropylene-steel fibre reinforced concrete. Cement and Concrete Research, 30, 63-69.

[64] Nematollahzade, M., Tajadini, A., Afshoon, I., Aslani, F., 2020. Influence of different curing conditions and water to cement ratio on properties of self-compacting concretes. Construction and Building Materials, 237, 117570.

[65] Ferraz, J.M., Menezzi, C., Texeira, D., Martins, S., 2011. Effects of treatment of coir fiber and cement/fiber ration on properties of cement-bonded composites. Bioresources, 3, 3481-3492.

[66] Rashid, M.U., 2020. Experimental investigation on durability characteristics of steel and polypropylene fiber reinforced concrete exposed to natural weathering action. Construction and Building Materials, 250, 118910.

[67] Moradikhou, A.B., Esparham, A., Avanaki, M.J., 2020. Physical & mechanical properties of fiber reinforced metakaolin-based geopolymer concrete. Construction and Building Materials, 251, 118965.

[68] Kasagani, H., Rao, C.B.K., 2018. Effect of graded fibers on stress-strain behavior of glass fiber reinforced concrete in tension. Construction and Building Materials, 183, 592-604.

[69] Liu, X., Wu, T., Liu, P., 2019. Stress-strain relationship for plain and fiber-reinforced lightweight aggregate concrete. Construction and Building Materials, 225, 256-272.

[70] Hongbo, Z., Haiyun, Z., Hongxiang, G., 2020. Characteristics of ductility enhancement of concrete by a macro polypropylene fiber. Results in Materials, https://doi.org/10.1016/j.rinma.2020.100087.

[71] Cao, S., Yilmaz, E., Song, W.D., 2019. Fiber type effect on strength, toughness and microstructure of early age cemented tailings backfill. Construction and Building Materials, 223, 44-54.